Spatiotemporal Temperature Patterns During Hydrogen Oxidation on a Nickel Disk

Samuel L. Lane, Michael D. Graham, and Dan Luss
Dept. of Chemical Engineering, University of Houston, Houston, TX 77204

Spatiotemporal temperature patterns on a polycrystalline nickel disk were recorded using infrared video imaging during atmospheric hydrogen oxidation and characterized by the proper orthogonal decomposition pattern analysis technique. The system was studied at two different residence times, 3.2 s and 6.4 s. At moderate feed temperatures, steady-state multiplicity and rate oscillations were found. Oscillations at a residence time of 6.4 s were periodic and essentially spatially uniform. At a residence time of 3.2 s, however, the surface temperature became nonuniform, and rate oscillations occurred via traveling temperature waves which emanated from "pacemakers" (locally active regions) on the edge of the catalyst. During periodic oscillations, the waves were emitted synchronously from the pacemakers, while during chaotic oscillations, the pacemakers were desynchronized and emitted waves independently of each other. Nonlocal gas-phase coupling between distance surface elements caused spatial desynchronization during rate oscillations.

Introduction

Spatiotemporal concentration and temperature patterns have been observed in a wide variety of chemically reacting systems since Turing (1952) originally predicted their existence four decades ago. These patterns may form spontaneously by a "symmetry breaking" bifurcation caused by the nonlinear interaction between the chemical kinetics and the transport processes (Turing, 1952; Prigogine and Nicolis, 1967; Prigogine and Lefever, 1968). The well-known Belousov-Zhabotinskii homogeneous reaction system (Zaiken and Zhabotinskii, 1970) exhibits a wide variety of spatiotemporal concentration patterns, such as rotating spirals and traveling waves. Several theoretical studies have predicted that spatiotemporal patterns exist also on heterogeneous catalytic surfaces (Pismen, 1980; Sheintuch, 1981; Schmitz and Tsotsis, 1983). Experimental studies revealed intricate concentration patterns including rotating spirals, "target patterns," and solitary plane waves on single platinum crystal surfaces during low-pressure CO oxidation (Jakubith et al., 1990; Ertl, 1991) and NO reduction with NH_3 (Veser et al., 1992) under UHV conditions. However, industrial catalytic systems (polycrystalline, supported catalysts at high pressures) are inherently nonuniform, and their spatiotemporal behavior usually differs from the simple types mentioned above. Infrared video imaging (thermography) has been used to detect and measure temperature patterns in several of these catalytic systems. Brown et al. (1985) found that reaction rate oscillations on polycrystalline platinum catalysts during hydrogen oxidation were due to the formation and fluctuation of locally active "hot spots." Kellow and Wolf (1990, 1991) found hot spots on a Rh/SiO_2 wafer during the oxidation of ethylene, which changed their shape and size as they moved across the catalyst. Lobban and Luss (1989) found that propagating temperature waves caused rate oscillations during hydrogen oxidation on a polycrystalline nickel catalyst. They noted that temperature waves always propagated from one of several active points (pacemakers) on the edge of the catalyst.

The idea that propagating reaction fronts may originate at local heterogeneities (pacemakers) was proposed by Langmuir (1921). He noted that the edges of an adsorbed film are much more susceptible to chemical action and that "the film would be removed progressively from its bounding edge inward." Experimental evidence of this concept was given by scanning LEED of a platinum surface during CO oxidation (Cox et al., 1985; Imbihl et al., 1986). Propagating waves of structure transformations were observed to usually emanate from the surface edges, where there was a higher defect density. Numerical simulations by Imbihl et al. (1985) showed that waves were repeatedly emitted from the surface edges into the bulk.

Correspondence concerning this article should be addressed to D. Luss.

Pacemakers for CO oxidation were produced on a platinum surface by locally irradiating a small spot on the surface with a laser pulse (Fink et al., 1989). Experiments showed that a circular reaction front propagated outward from the pacemaker.

Reaction rate oscillations during hydrogen oxidation on nickel catalysts have been studied by many researchers (Belyaev et al., 1973; Schmitz et al., 1979, 1980; Kurtanjek et al., 1980; Tsitsopoulos and Tsotsis, 1987). Reviews of hydrogen oxidation kinetics by Norton (1982) and Ertl (1983) suggest that the reaction proceeds via a Langmuir-Hinshelwood mechanism. Kurtanjek et al. (1980) used a CPD (contact potential difference) technique to follow the state of the nickel surface during oscillations, showing that the reaction rate decreases upon surface oxidation and increases upon reduction. Reaction rate oscillations may arise due to the cyclic oxidation and reduction of the nickel surface. Tsitsopoulos and Tsotsis (1987) confirmed this oxidation/reduction oscillatory mechanism by *in-situ* ellipsometry measurements of the nickel surface. In both studies, isothermal oscillations were found, indicating that hydrogen oxidation kinetics on nickel are inherently oscillatory. Chaotic rate oscillations were found in nonisothermal experiments by Schmitz et al. (1979). A mathematical model by Schmitz's group (1980) describing nonisothermal oxidation-reduction kinetics predicted chaotic oscillations similar to those observed experimentally.

Previous models of oscillatory behavior were usually based on the assumption that the surface concentrations and temperature are spatially uniform. Experimental evidence shows that this assumption is often invalid. The gas phase adjacent to the catalytic surface may transmit information among distant surface elements. This coupling mechanism may be either autocatalytic or inhibitory. The inhibitory case may introduce spatial desynchronization on catalytic surfaces, as discussed by Eiswirth et al. (1989).

We report here on the impact of feed temperature, feed concentration, and average residence time on surface temperature patterns on a thin nickel catalytic disk during hydrogen oxidation rate oscillations. The goal is to enhance our understanding of the factors leading to the evolution of nonuniform temperature patterns and to properly classify them.

Experimental System

The experiments were conducted in a cylindrical aluminum reactor with an inner diameter of 7.0 cm and a depth of 3.8 cm (Figure 1). The reactor lid was an infrared-transparent sapphire window (Union Carbide Crystals Division) which allowed viewing of the catalyst during reaction. The window was sealed by a stainless-steel clamping frame. The reactor was operated at atmospheric pressure and placed inside an insulated oven [14 in. × 14 in. × 12 in. (356 mm × 356 mm × 305 mm)], heated by a cylindrical heating element. A PID temperature controller (Omega CN2041) kept the inlet gas temperature to within 0.1°C of the setpoint. The catalyst was a circular disk of polycrystalline nickel (99.0%, A. D. Mackay) of 3.8 cm diameter and 0.13 mm thickness. It was held horizontally in the center of the reactor by four thermocouple wires (Iron-Constantan), which were placed through four small holes (0.8 mm dia.) drilled near the catalyst edge. A fifth thermocouple was placed under the center of the disk. Thermocouple readings were digitized and recorded at frequencies of 1–10 Hz. The catalyst was activated by alternately oxidizing and reducing it for several 24 hour periods at 400°C.

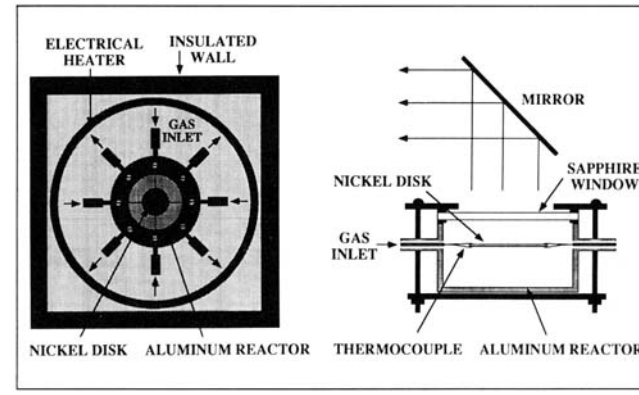

Figure 1. Experimental setup viewed from the top (left) and side (right).

The feed gases used were prepurified-grade hydrogen (99.99%, Linde) and extra-dry-grade oxygen (99.6%, Linde). The gases were further purified with an in-line purifier (Molecular Sieve 4A, Linde) to remove any moisture in the feed. Gas flow rates were controlled by Tylan FC-280S mass-flow controllers. The gases were premixed in a glass bead bed and fed to the reactor through four inlet ports. The product gases exited the reactor through four outlet ports. Tracer analysis confirmed that the reactor's residence time distribution was similar to that of a CSTR.

A liquid-nitrogen-cooled infrared video camera (AGEMA Thermovision 780) produced an 128×64 matrix of local radiation levels which were converted into local surface temperature images. It was necessary to operate the camera horizontally, so a mirror was used to view the catalyst. A 5.6 cm by 4.6 cm field was scanned by the camera which produced a spatial resolution of 0.3 mm^2. Radiation levels were measured with eight-bit accuracy giving a typical temperature accuracy of 0.2°C. The camera scanned the field 25 times per second, but data recording limitations allowed for only 6.25 images per second to be digitized and recorded. Temperature images were displayed in real time on a color monitor, as well as being saved on a Mac II computer for later analysis. Effluent gas stream concentrations of oxygen, hydrogen and water were continuously measured by a mass spectrometer (Dycor MA200M) with a typical frequency of 1 Hz.

The two main parameters varied in the experiments were the feed temperature, T_f, and the oxygen feed concentration, C_{O_2}. The experiments were conducted by making small step changes in either T_f or C_{O_2} while keeping the other parameters constant. After making a change, the reactor was allowed to equilibrate (usually overnight) to the new condition. Some of the previous studies of hydrogen oxidation on nickel (Kurtanjek et al., 1980; Lobban and Luss, 1989) were conducted by running a series of experiments (changing T_f or C_{O_2}), and then leaving the reactor in a reducing atmosphere (100% H_2, $T_f = 450$°C) between experiments for reactivation. It was found, however, that this mode of operation led to reproducibility problems. After "reactivation," the reactor behavior (such as temperature patterns and frequency of oscillations) continued to change for at least 24 hours. In an effort to avoid collecting

transient data, the system was run continuously (sometimes for months at a time) without stopping for reactivation. This continuous operation was possible because steady-state conversions did not change with catalyst age.

Spatiotemporal Pattern Characterization

To elucidate the observed patterns in a clear, objective and quantitative manner, we employed the statistical pattern recognition technique of the proper orthogonal decomposition (POD), also known as Karhunen-Loeve decomposition (Lumley, 1970; Fukunaga, 1990). Given an ensemble of instantaneous measurements, the technique yields an optimal orthogonal basis for the representation of the ensemble and a measure of the relative contribution of the basis functions (modes) to the total "energy" (mean square fluctuation in time) of the ensemble. The basis is optimal in the sense that a truncated series representation has a smaller mean square truncation error than a representation by any other basis. That is, the signal $u(x,t)$ has an optimal N term series representation:

$$u(x,t) = \sum_{i=1}^{N} a_i(t)\varphi_i(x), \tag{1}$$

where $\varphi_i(x)$ are the time-independent spatial modes and $a_i(t)$ are the time-dependent amplitudes, both determined by the POD. This is in contrast to other techniques such as Fourier analysis, where the basis functions are determined *a priori*. In data analysis, the amplitudes and modes are equally important, as the modes show the important spatial structures, and the amplitudes show how the structures interact in time. A more detailed description of our application of the POD technique is presented elsewhere (Graham et al., 1993).

The optimization problem for the basis functions reduces to the eigenvalue problem:

$$\langle \overline{u(x,t)u(x',t)}\varphi_i(x')\rangle = \lambda_i\varphi_i(x), \tag{2}$$

where the overbar represents a time average and the angle brackets represent integration over the spatial domain. The eigenvalue λ_i associated with each mode φ_i shows the magnitude of the contribution of that mode to the overall pattern, in the mean square sense. It thus gives a measure of the "energy" of the corresponding mode. We normalize the eigenvalues by dividing each by the total energy (sum of all the eigenvalues). The eigenvalue problem is efficiently solved using the "method of snapshots" (Sirovich, 1987; Sirovich and Sirovich, 1989). The POD modes are orthogonal in space,

$$\langle \varphi_i(x)\varphi_j(x)\rangle = \delta_{ij}, \tag{3}$$

and the amplitudes are orthogonal in time,

$$\overline{a_i(t)a_j(t)} = \lambda_j\delta_{ij}. \tag{4}$$

The POD has a number of important characteristics that make it particularly useful for data analysis.

1. It provides a natural ordering of the time-independent spatial structures by a measure of their relative contribution to the pattern.

2. Unimportant structures (noise, experimental artifacts, and so on) are easily recognizable and can be neglected, thus simplifying the analysis.

3. Splitting the spatiotemporal pattern into a series of stationary patterns and corresponding time-dependent amplitudes simplifies presentation and classification of the data.

Experimental Results

Experiments were carried out initially to determine and classify the temporal behavior of the reactor, to determine the various observable bifurcations (transitions) from qualitatively different dynamic behaviors and to construct a map of the bifurcations in the feed temperature vs. feed concentration plane. We later used infrared imaging to examine the spatial surface temperature in the parameter region in which the reactor exhibited oscillatory behavior.

Temporal reactor dynamics

The influence of the feed temperature (T_f) and oxygen feed concentration (C_{O_2}) on the temporal dynamics of the reactor was studied at two residence times, τ, of 3.2 s and 6.4 s. At both residence times, ignited and extinguished steady states existed, along with a variety of time-dependent behavior. At each residence time, a series of bifurcation diagrams of oxygen conversion vs. feed temperature or oxygen feed concentration were constructed to map out regions of qualitatively different behavior. Figures 2a-2c show the dependence of the oxygen conversion on T_f at C_{O_2} of 1%, 2% and 5% by vol., and a residence time of 3.2 s. At C_{O_2} of 1% by vol., three different regions are found. For $T_f < 190°C$, only an extinguished (E), low-conversion state existed. For $T_f > 194°C$, only an ignited (I), high-conversion state existed. In the narrow intermediate region, steady-state multiplicity existed with branches of stable ignited and extinguished states ($I+E$). The transition between the upper and lower branches (ignition or extinction) occurred at saddle-node bifurcation points. This steady-state multiplicity is a common feature of highly exothermic reactions in a CSTR. At $C_{O_2} = 2\%$ by vol., a similar bistable situation existed, but in addition, stable periodic oscillations existed on a portion of the upper branch. These oscillations originate at two Hopf bifurcation points and create two new types of phase-plane behavior not observed at $C_{O_2} = 1\%$. For $184°C < T_f < 194°C$, the catalyst attained either an extinguished or a periodic oscillatory state ($P+E$). For $194°C < T_f < 200°C$, only periodic oscillations (P) existed. At $C_{O_2} = 5\%$, stable chaotic oscillations (C) existed in addition to periodic oscillations. Both chaotic oscillations and extinguished states ($C+E$) were stable for T_f between 167°C and 196°C. The periodic oscillations disappear at a feed temperature of 148°C via a saddle node of a periodic orbit (SNP) bifurcation. This extinction could also have occurred via a saddle-loop bifurcation, but analysis of the various bifurcation lines in the bifurcation map (see inset in Figure 5) strongly suggests that this is a SNP bifurcation.

The temperature variations at one point on the disk (12 o'clock with reference to the figures presented later) are shown in Figure 3 for two reactor feed temperatures ($C_{O_2} = 5\%$, $\tau = 3.2$ s). At $T_f = 165°C$ (Figure 3a), periodic relaxation oscillations are found with a period of about 3,800 s. They are characterized by a slow temperature rise leading to a rapid temperature jump lasting for about 40 s, followed by a period of slow gradual

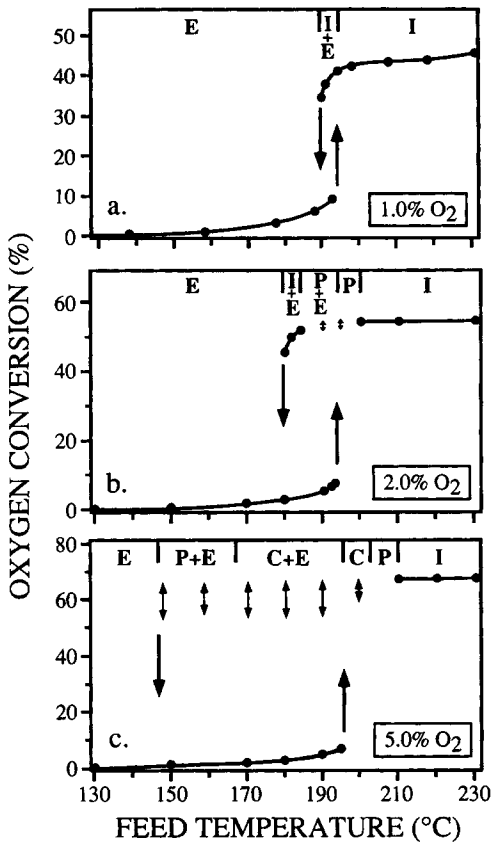

Figure 2. Bifurcation diagrams showing the dependence of oxygen conversion on the gas feed temperature at $\tau = 3.2$ s.

The respective oxygen feed concentrations are: a) 1.0%, b) 2.0%, and c) 5.0%.

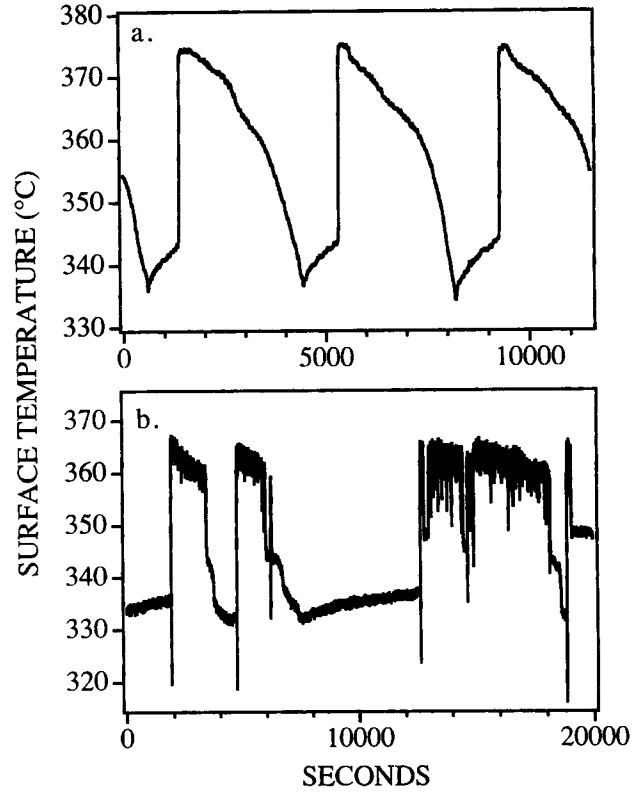

Figure 3. Time series of the surface temperature at the 12 o'clock position during a) periodic ($T_f = 165$°C) and b) chaotic ($T_f = 175$°C) rate oscillations; $C_{O_2} = 5.0\%$ and $\tau = 3.2$ s.

cooling for nearly an hour. The chaotic oscillations at $T_f = 175$°C (Figure 3b) also have a long timescale trend, but additionally exhibit small, rapid, aperiodic oscillations (~5°C, period 1.6 s) and large downward spikes (15–30°C, duration ~50 s). The transition from the periodic to chaotic oscillations occurred rapidly, and we were not able to identify or classify the transition scenario.

Figure 4 is a bifurcation diagram of oxygen conversion vs. feed concentration at a feed temperature of 190°C and a residence time of 3.2 s. Once again, an extinguished steady state coexisted with either periodic ($P+E$) or chaotic ($C+E$) oscillations or an ignited steady state ($I+E$). When C_{O_2} was lowered to 1%, the ignited steady state extinguished via a saddle-node bifurcation. Note that in this case the low-conversion state could only be ignited by increasing the feed temperature (above 194°C) and not by changing the oxygen concentration.

The bifurcation diagrams were used to construct a bifurcation map (Figure 5a) in the T_f vs. C_{O_2} plane for $\tau = 3.2$ s. It maps the location and organization of seven regions with qualitatively different behavior, bounded by four bifurcation lines. The solid line denotes saddle-node bifurcations, and the dotted line denotes saddle nodes of periodic orbits (SNP). These two lines form a cusp which bounds the region of multiple stable states. The dashed line denotes a Hopf bifurcation, that is, a transition from a stationary state to a periodic oscillation. The dashed-dotted line denotes the transition from periodic to chaotic oscillations. The inset is provided to clarify the bifurcations in the region where the saddle node, SNP, and Hopf bifurcation lines converge. The bifurcation map at a residence time of 6.4 s (Figure 5b) is qualitatively similar to that at $\tau = 3.2$ s, with both maps containing a cusp bounding the multiplicity region and a Hopf bifurcation line. The size and relative position of these regions depend on the residence time. The multiplicity cusp at a τ of 6.4 s is smaller than that at a τ of 3.2 s and shifted to higher oxygen feed concentrations. This change

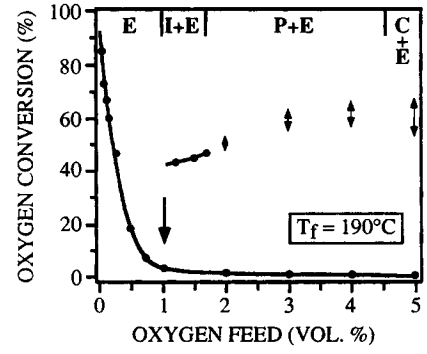

Figure 4. Bifurcation diagram showing the dependence of oxygen conversion on the oxygen feed concentration at $T_f = 190$°C and $\tau = 3.2$.

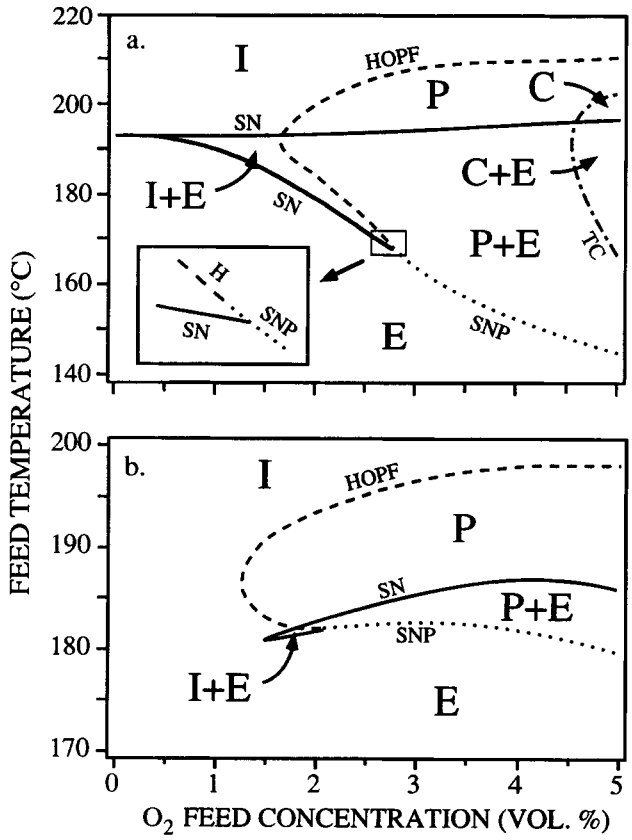

Figure 5. Bifurcation maps showing the regions of qualitatively different reactor behavior for residence times of a) 3.2 s and b) 6.4 s.

The lines outline the bifurcations between the different regions: I = ignited steady states; E = extinguished steady states; P = periodic oscillations; and C = chaotic oscillations. The four lines mark the (SN) saddle-node bifurcations (———), Hopf bifurcations (— —), saddle node (SNP) of periodic orbits (· · · ·), and the (TC) transition to chaos (—·—·).

is probably due to the decreased heat generation at the higher residence time. The rate of heat generation equals the heat of reaction $(-\Delta H)$ times the product of the oxygen conversion and oxygen feed flow rate. When the residence time is doubled from 3.2 s to 6.4 s, the conversion increases from roughly 60% to 80%, but the oxygen flow rate is decreased by 50% (for fixed oxygen %). Therefore, the rate of heat generation at a τ of 3.2 s is approximately 50% larger than that at a τ of 6.4 s, which leads to the larger region of multiplicity observed at the shorter residence time. The increase of the multiplicity region with increased rate of heat generation is also the cause for the increase in the range of feed temperatures for which multiplicity occurs with increasing oxygen feed concentration (that is, the cusp becomes wider with increasing C_{O_2}). The higher oxygen feed concentrations increase the reaction rate and heat generation. It is surprising that for both residence times, the ignition (saddle-node) temperatures are rather insensitive to change in the oxygen feed concentration.

The shape of the Hopf bifurcation line at both residence times is similar, but its position changes as τ increases from 3.2 s to 6.4 s. The feed temperature range for which oscillations exist decreases from 147–210°C for $\tau = 3.2$ s to 180–198°C for $\tau = 6.4$ s. The limiting oxygen concentration above which oscillations occur also decreases slightly, from 1.7% to 1.2% with the increased residence time. The observed oscillations at $\tau = 6.4$ s were always periodic, and no transition to chaos was seen for oxygen concentrations below 5%. It is possible that chaotic oscillations existed for higher oxygen concentrations; however, this possibility was not explored as 5% O_2 in H_2 is the explosion limit of this mixture.

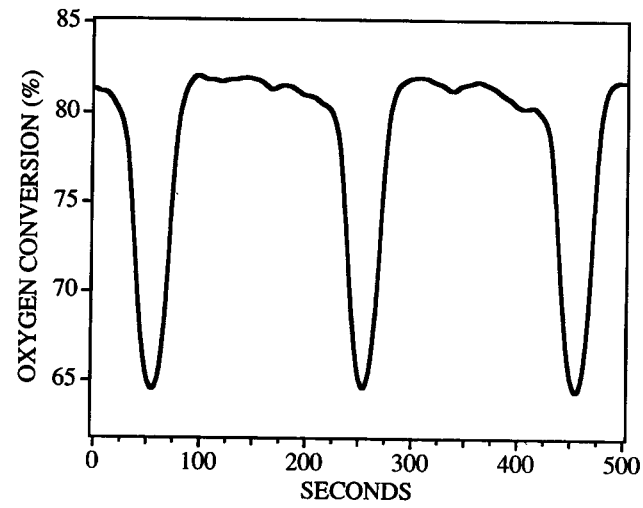

Figure 6. Oscillations in oxygen conversion during a periodic state at $T_f = 194$°C, $C_{O_2} = 3.0$%, and $\tau = 6.4$ s.

For a residence time of 6.4 s, the cusp bounding the small $I+E$ region consists of ignition and extinction lines which are positively sloped. According to Harold et al. (1987), this implies that the isothermal reaction rate is of negative order with respect to oxygen for some concentrations. We caution against using the slopes to draw this conclusion as the sign of the slope of the short extinction branch is very sensitive to experimental errors as the accuracy of the points is about ±1°C. Similarly, the local maximum in the ignition (*SN*) line in Figure 5b suggests that an isolated branch of extinguished states exists in a bifurcation diagram of rate vs. oxygen feed concentration at a feed temperature of about 185°C. Again, we caution that the local maximum may be due to experimental errors in determining this line. No such isolated extinguished branch was observed.

Spatiotemporal temperature patterns on the catalyst

The infrared camera was used to determine the spatial catalyst surface temperature when the rate was oscillatory. For a residence time of 6.4 s, the catalyst surface temperature was always essentially uniform during the rate oscillations. Figure 6 is an example of typical periodic oscillations in the oxygen conversion at $\tau = 6.4$ s ($T_f = 194$°C, $C_{O_2} = 3.0$%). The oscillation is characterized by a sharp downward peak lasting about 65 s, followed by a long, high-conversion period of about 140 s. Six thermal images of the catalyst surface temperature during one of the downward peaks (temperature changes very little during the high-conversion section) are shown in Figure 7. The local surface temperature is represented by a gradual color transition from red to blue with red being 267°C and blue being 248°C in this example. Visual inspection shows that while the temporal surface temperature variations are very large, the

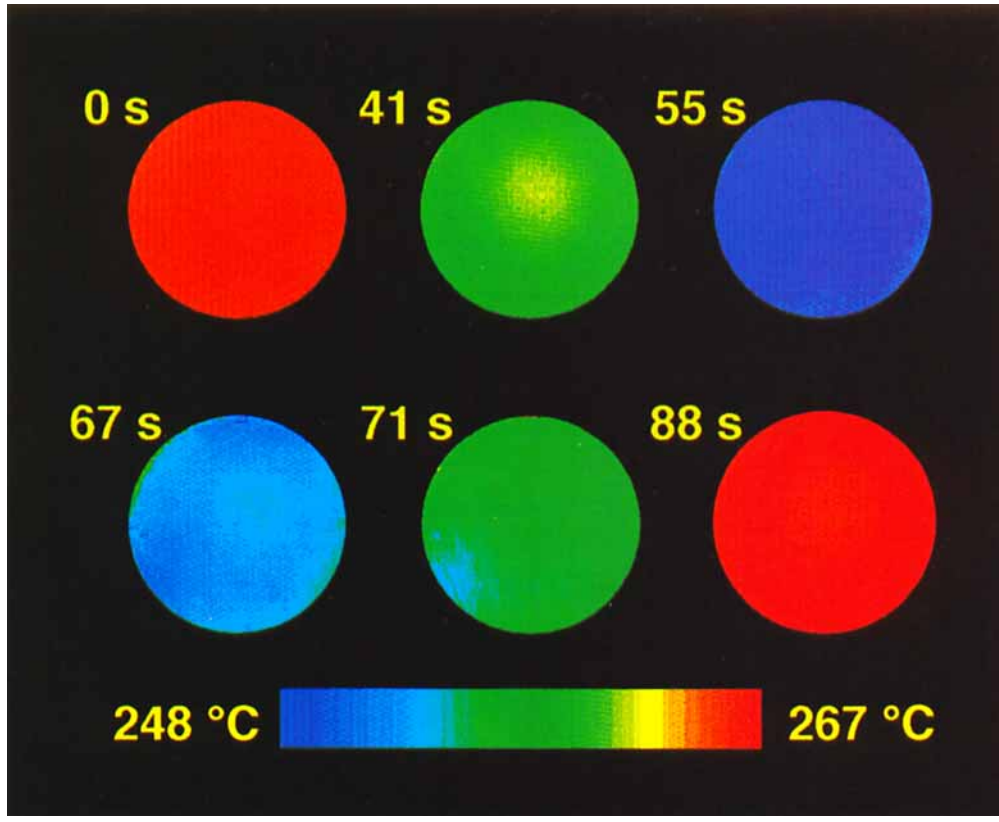

Figure 7. Six thermal images of the catalyst surface during the first downward peak in Figure 6.

The local temperature is represented by the gradual color transition from red to blue. Red represents the highest temperature (267°C) and blue represents the lowest (248°C). Times are in s.

spatial variations are quite small. A POD analysis of two periods of the oscillation using 40 snapshots from a sequence of 2,400 images (6.25 Hz) was done to quantify the spatial uniformity of the oscillations. The three most important spatial modes $\varphi_i(x,y)$, their energies λ_i, and amplitudes $a_i(t)$, $i=1-3$, are shown in Figure 8. The modes represent the temperature deviation from the time-average pattern, with red indicating the largest positive deviation from the mean and blue, the largest negative deviation. The contribution of a mode to the temperature at a point (x,y) on the disk is the product $a_i(t)\varphi_i(x,y)$. The first mode, $\varphi_1(x,y)$, is uniform with almost no spatial dependence and corresponds to homogeneous heating and cooling of the surface. This mode is by far the most dominant, containing 98.7% ($\lambda_1=0.987$) of the energy (mean square fluctuation) in the system. The POD confirms the visual observation that the oscillations are essentially spatially uniform at $\tau=6.4$ s and quantifies the degree of homogeneity as 98.7%. The amplitude of mode 1, $a_1(t)$, almost exactly mirrors that of the reactor conversion (Figure 6), which is not surprising since mode 1 contains nearly all of the energy of the system. The small, nonuniform component of the oscillation is made up of modes 2 and 3, which together contribute only 1.0% of the energy. Mode 2 contains a temperature maximum near the center of the disk, and mode 3 contains a maximum near the upper right edge and a minimum near the center. Despite the fact these modes have clear spatial structure, they contribute very little to the pattern because of their small energies. These modes do, however, show the utility of the POD technique in quantitatively detecting the presence of small spatial structures which may not be visible to the eye. The contribution of modes 4 and higher is negligible (<0.3%) and is largely dominated by noise.

Thermal images of the catalyst surface at $\tau=3.2$ s showed

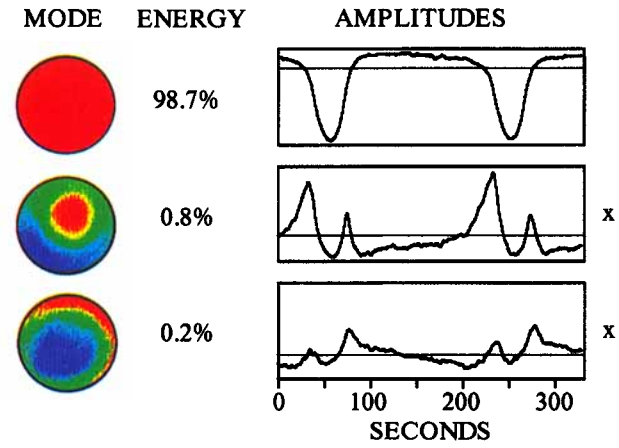

Figure 8. The three most dominant POD modes $\varphi_i(x,y)$, their energies, and temporal amplitudes $a_i(t)$, $i=1-3$; $T_f=194$°C, $C_{O_2}=3.0$%, and $\tau=6.4$ s.

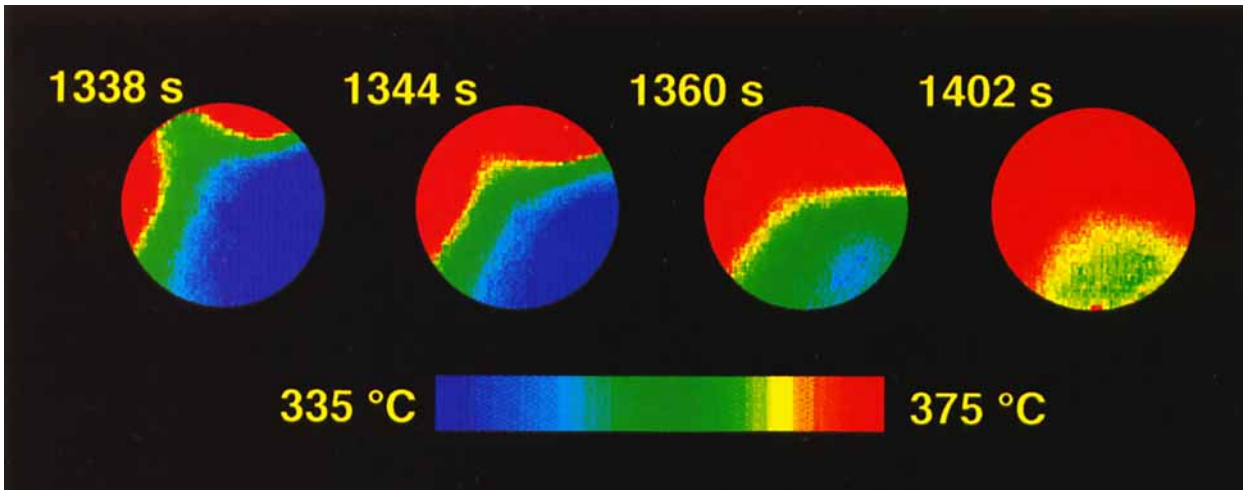

Figure 9. Sequence of four temperature profiles during the periodic oscillation in Figure 3a.

The sequence shows two fronts propagating away from pacemakers at 9 and 1 o'clock, and then coalescing and propagating as one front.

that the surface temperature was no longer uniform, and traveling temperature fronts existed during periodic and chaotic oscillations. We describe here three such cases, with increasing degree of spatial complexity, conducted at $C_{O_2} = 5.0\%$ and various feed temperatures. The POD of two of these cases ($T_f = 165°C$ and 175°C) were analyzed in Graham et al. (1993). At $T_f = 165°C$, periodic relaxation oscillations exist, as shown in Figure 3a. The oscillations are characterized by a slow temperature rise leading to a rapid temperature jump of about 30°C lasting for about 40 s, followed by slow gradual cooling for nearly an hour. Infrared imaging shows that during the rapid temperature jump, two temperature fronts form at pacemakers located at 9 o'clock and 1 o'clock (Figure 9, 1,338 s). The two fronts propagate outward, and then coalesce and propagate as one front across the remainder of the surface. The origin of the pacemakers is unknown, but is most likely related to the inherent inhomogeneity of the disk and the impact of the supports, as both pacemakers are located at the edge of the disk, near one of the supports.

A POD analysis over one period of this oscillation was carried out using 40 snapshots from a sequence of 6,000 images (1.56 Hz). The three most important spatial modes, their energies, and amplitudes are shown in Figure 10. Most of the energy is contained in the first and second modes which contain 88% and 10% of the energy, respectively. Only 2% of the energy is distributed among the remaining 38 modes. The two localized temperature maxima in mode 2 clearly correspond to the two pacemakers seen in Figure 9. The highest values of mode 1 are also centered around the two pacemakers, but decrease more gradually away from the pacemakers than in mode 2. Analysis of the temporal amplitudes, $a_1(t)$ and $a_2(t)$, explains the interaction between modes 1 and 2. The amplitude of mode 2 has a sharp positive spike near $t = 1{,}300$ s. This corresponds to the rapid formation of the two temperature fronts shown in Figure 9 ($t = 1{,}338$ s). The following positive step increase in the amplitude of mode 1 corresponds to a more diffuse heating away from the pacemakers. Thus, the interaction of these two modes accounts for the formation of the two fronts and their propagation across the surface. The velocity of the front propagation was about 0.1 cm/s, which is consistent with motion due to thermal conduction (trigger waves). The relevant time and length scales for the thermal response of the disk are:

$$\tau_{hs} = \frac{\rho c_p}{h a_v} = 15 \text{ s}, \tag{5}$$

and

$$L_{hs} = \sqrt{\frac{k}{h a_v}} = 1.5 \text{ cm}, \tag{6}$$

where $h = 20.1$ J/m^2·s·K is the experimentally determined heat-transfer coefficient, $a_v = 1.51 \times 10^4$ m^{-1} is the surface to volume ratio of the disk, $\rho c_p = 4.5 \times 10^6$ J/m^3·K, and $k = 72$ W/m·K is the thermal conductivity of nickel. The velocity of a thermal front propagating via thermal conduction is of the order of

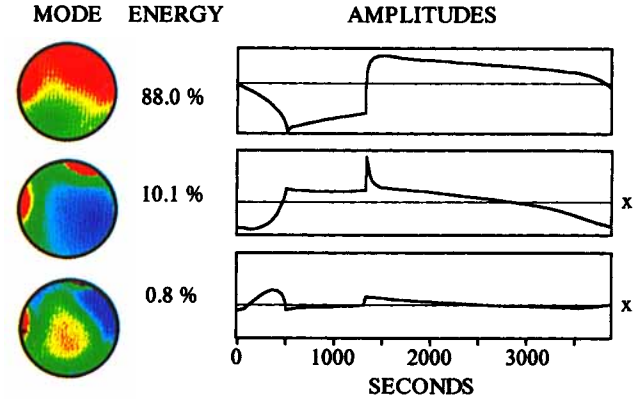

Figure 10. Three most dominant POD modes $\varphi_i(x,y)$, their energies, and temporal amplitudes $a_i(t)$, $i = 1$-3; $T_f = 165°C$, $C_{O_2} = 5.0\%$, and $\tau = 3.2$ s.

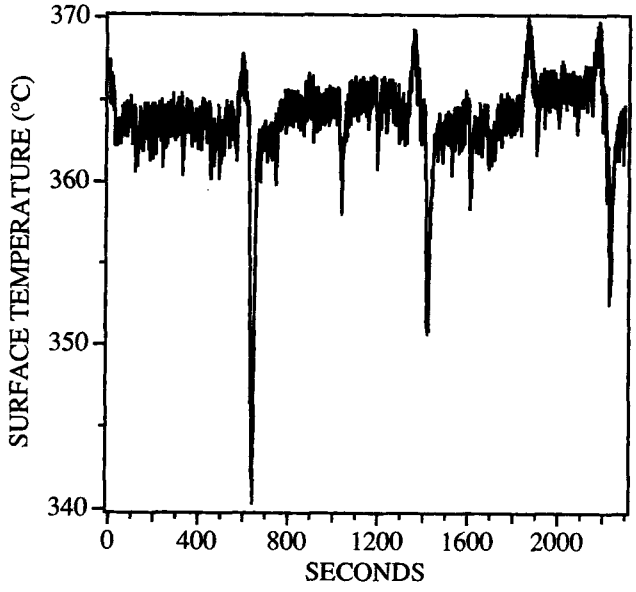

Figure 11. Chaotic temperature fluctuations at the 12 o'clock position during a high-temperature interval, $T_f = 175°C$, $C_{O_2} = 5.0\%$, and $\tau = 3.2$ s.

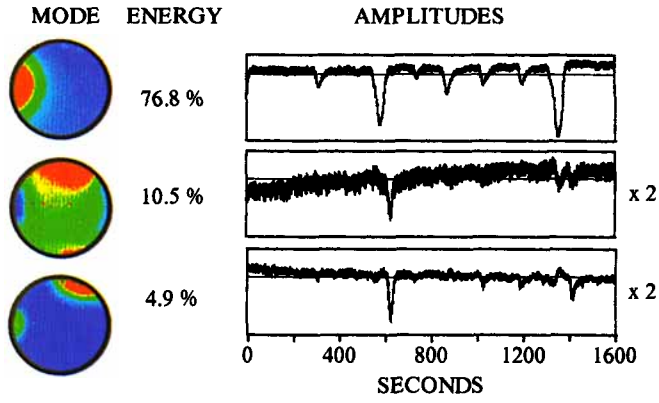

Figure 12. Three most dominant POD modes $\varphi_i(x,y)$, their energies, and temporal amplitudes $a_i(t)$, $i = 1$-3; $T_f = 175°C$, $C_{O_2} = 5.0\%$, and $\tau = 3.2$ s.

Samples were taken during the entire interval shown in Figure 11.

the ratio L_{hs}/τ_{hs}. This value is 0.1 cm/s for the disk and agrees well with the experimentally observed value. Therefore, the spatiotemporal behavior under these conditions can be characterized by periodic formation of fronts at two pacemakers and subsequent front propagation due to thermal conduction (trigger waves).

When the feed temperature is increased to 175°C ($\tau = 3.2$ s), chaotic oscillations occur (Figure 3b), consisting of small, rapid, aperiodic oscillations (~5°C, period 1.6 s), large downward spikes (15-30°C, duration ~50 s), and a slow oscillation (~40°C, period >1,000 s). The slow oscillation is somewhat similar to that at 165°C, but the rapid oscillations and spikes are new features. They occur when the average surface temperature is highest (~365°C, Figure 3b). A typical chaotic fluctuation of the 12 o'clock thermocouple signal (Figure 11) during the high-temperature section includes three large downward spikes, each preceded by a small upward spike and a background of rapid, small fluctuations. Thermal images were recorded over the first 1,600 s of this interval (10,000 images, 6.25 Hz), and a POD analysis was completed using 65 snapshots (Figure 12). Modes 1 and 2 consist of temperature maxima at the 9 o'clock and 1 o'clock pacemakers, respectively. Since each pacemaker now corresponds to a different mode, the synchrony found at $T_f = 165°C$ is no longer dominant (mode amplitudes are orthogonal in time and thus unsynchronized).

The large negative spike in the amplitude of mode 1 (Figure 12, $t = 600$ s), corresponds to a cooling front propagating from the 9 o'clock pacemaker. This spike is immediately followed by a large negative spike in the amplitude of mode 2, corresponding to a cooling front propagating from the 1 o'clock pacemaker. Eight thermal images showing the propagation of these two cooling fronts are shown in Figure 13. Initially, the 9 o'clock pacemaker produces a cooling front which propagates about 40% across the disk and then retreats. Then, the 1 o'clock pacemaker produces a cooling front which moves about 30% across the disk before retreating. Fronts created at the 1 o'clock pacemaker were always preceded by fronts created at the 9 o'clock pacemaker, but the converse was never observed. In addition, the 1 o'clock pacemaker was triggered only by sufficiently large spikes at the other pacemaker. The asynchronous propagation of fronts from the two pacemakers was typical of the chaotic oscillations observed at $T_f = 175°C$.

An important point to note is that a cooling front from one pacemaker coincides with heating on the rest of the catalyst. This can be seen in the thermal images as well as in the 12 o'clock thermocouple time series (Figure 11). The temperature at 12 o'clock increases due to the propagation of a cooling front from 9 o'clock, just before decreasing due to the cooling front formation at 1 o'clock. This behavior is attributed to gas-phase coupling: that is, a large decrease in temperature (reaction rate) at the 9 o'clock pacemaker increases the gas-phase oxygen concentration which increases the reaction rate (temperature) on the rest of the disk.

At a feed temperature of 195°C ($\tau = 3.2$ s), the complexity and frequency of the oscillations increase as both rapid heating and cooling fronts are formed. These fronts propagate from three different pacemakers located at 9, 1, and 6 o'clock. Cooling fronts typically propagated from the 6 and 9 o'clock pacemakers, while heating fronts usually propagated from the 1 o'clock pacemaker, although this was not always the case. Front propagation from the 6 and 9 o'clock pacemakers often was synchronized, but rarely did either of these pacemakers produce fronts synchronously with the 1 o'clock pacemaker. Eight thermal images of the catalyst during this rapidly changing pattern are shown in Figure 14. The first two images show cooling fronts propagating from the 6 and 9 o'clock pacemakers, followed by a heating front from the 1 o'clock pacemaker which propagates half way across the surface. Images 3-6 show the propagation of cooling fronts from the 6 and 9 o'clock pacemakers, which coalesce into one front and then separate into two distinct fronts. Images 7 and 8 show the propagation of another heating front from the 1 o'clock pacemaker.

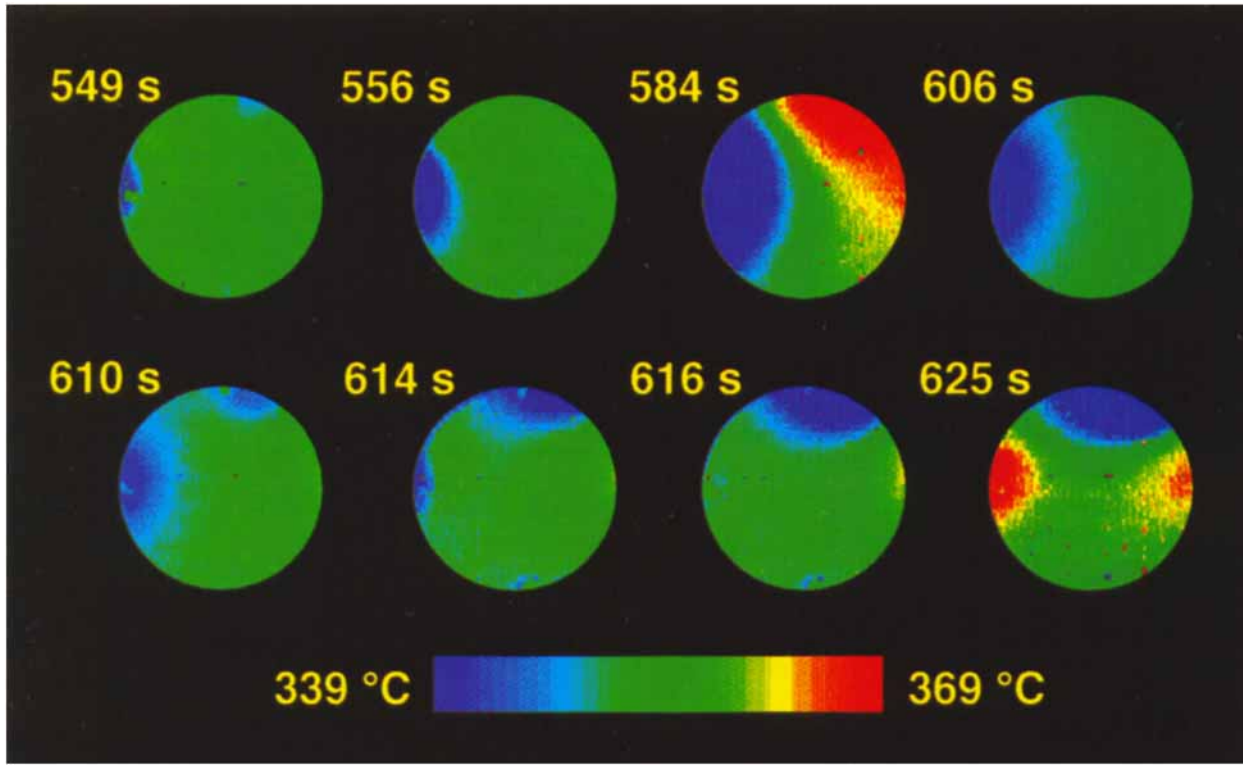

Figure 13. Eight thermal images of the catalyst recorded during an interval of the chaotic oscillations shown in Figure 11.

The sequence shows the propagation of a cooling front at the 9 o'clock pacemaker, which in turn triggers the propagation of a cooling front from the 1 o'clock pacemaker.

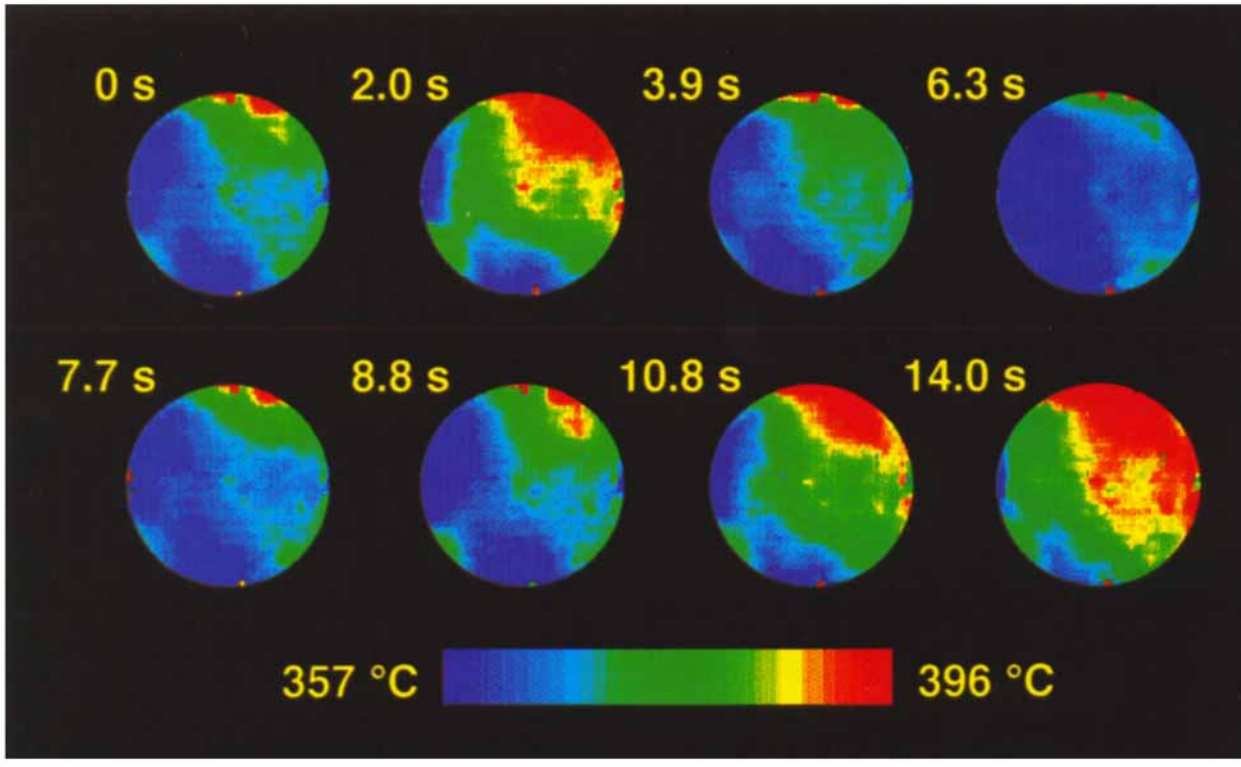

Figure 14. Eight thermal images of the catalyst recorded during chaotic oscillations at $T_f = 195°C$, $C_{O_2} = 5.0\%$, and $\tau = 3.2$ s.

The sequence shows the propagation of cooling fronts from the 6 and 9 o'clock pacemakers as well as heating fronts from the 1 o'clock pacemaker.

Table 1. Energies of the First Four POD Modes for Periodic Oscillations at Residence Times of 3.2, 6.4 and 12.8 s

Mode No.	$\tau = 3.2$ s	$\tau = 6.4$ s	$\tau = 12.8$ s
1	88.0%	98.7%	99.7%
2	10.1%	0.8%	0.16%
3	0.8%	0.2%	0.04%
4	0.4%	0.05%	0.03%

Discussion

The experiments show that the occurrence of spatial temperature patterns depends strongly on the average residence time in the CSTR. At a residence time of 3.2 s, the surface temperature had large spatial variations and rate oscillations occurred via propagating temperature fronts. At a residence time of 6.4 s, surface temperature oscillations were essentially uniform. In an additional experiment, at an average residence time of 12.8 s ($T_f = 198$°C, $C_{O_2} = 3.0\%$), surface temperature oscillations were even more spatially uniform than at 6.4 s, with the energy of the uniform mode increasing from 98.7% to 99.7%. This was the highest level of uniformity observed. The deviation from 100% is most likely due to noise, which was typically 0.2–0.3%. Table 1 summarizes the energies of the first four modes for periodic oscillations at $\tau = 3.2$, 6.4 and 12.8 s. It shows that at a high average residence time, the oscillations are very uniform, but as the average residence time is decreased, the oscillations become increasingly nonuniform and more energy is distributed among the nonhomogeneous modes. Onken and Wolf (1988) also observed that temperature oscillations during ethylene oxidation on Pt/SiO_2 wafers became increasingly nonuniform with decreasing residence time. They noted that surface temperature oscillations at two active catalyst spots were nearly identical at a high residence time, but oscillated asynchronously when the residence time was decreased by a factor of four.

The uniform temperature oscillations at the high average residence times are influenced strongly by the high thermal diffusion, which leads to a uniform surface temperature. A stability analysis of a reaction-diffusion system, in which only an autocatalytic variable diffuses, predicts that spatially uniform oscillations are the most unstable (Turing, 1952; Borckmans et al., 1990). In practice, the spatial temperature oscillations are not purely uniform, but propagate via very rapid "phase" waves. A slightly more active region of the catalyst initiates the oscillation and the rest of the surface rapidly follows (parts of the surface are slightly out of phase). Phase waves observed during the periodic oscillations at a residence time of 6.4 s propagated across the surface in about 2 s at a velocity of about 2 cm/s, which is about 20 times faster than that of the trigger waves.

At the residence time of 3.2 s, the surface temperature exhibited significant spatial variation, and uniform oscillations were not observed. Elmer (1988) showed that a nonlocal desynchronizing mechanism may change the stability of spatially uniform oscillations. The coupling of distant surface elements via the gas phase provides such a mechanism. An increase in the reaction rate (temperature) at one point on the surface decreases the gas-phase oxygen concentration leading to a decrease in the reaction rate (temperature) on the rest of the surface. This mechanism leads to spatial symmetry breaking and produces nonuniform temperature patterns on the catalyst surface. Nonuniform temperature profiles on an electrically heated platinum ribbon catalyst during ammonia oxidation were produced by a similar nonlocal desynchronizing mechanism (Lobban et al., 1989). Asymmetric temperature variations were produced when the average temperature (resistance) was held constant, because an increase in temperature (resistance) on one portion of the ribbon forced a decrease in temperature on another portion of the ribbon.

The impact of the gas-phase coupling tends to increase with decreasing residence time. It produces a desynchronizing effect through changes in the gas-phase oxygen concentration. Therefore, the impact of the gas-phase coupling depends on the magnitude of the change in the gas-phase oxygen concentration due to a local change in reaction rate. Consider a local decrease in surface activity (for example, due to surface oxidation) which creates a locally inactive region with low reaction rate. The corresponding increase in the oxygen concentration depends on the previous level of the reaction rate. The higher the reaction rate of the active state, the greater is the impact of the local deactivation. The reaction rate at a residence time of 3.2 s is roughly 50% higher than that at a residence time of 6.4 s (for constant C_{O_2}). Thus, the desynchronizing effect of the gas-phase coupling is stronger at the shorter residence time. This effect becomes even larger as the oxygen feed concentration is increased.

Thermal communication through the gas phase also provides a coupling between distant surface elements, but generates a *synchronizing* effect which minimizes nonuniformities in surface temperature. A local increase in reaction rate (temperature) at one point on the surface increases the gas-phase temperature leading to an increase in the reaction rate (temperature) on the rest of the surface. Thermocouple measurements of the gas-phase temperature showed that the magnitude of typical gas temperature fluctuations are in the range of 2–5°C.

To accurately model the spatial patterns, a model must account for the nonlocal coupling through the gas phase. In addition, it must be able to predict the bifurcations between the regions of qualitatively different behavior (Figure 5). Specifically, it is essential that the model can predict the "organizing centers" observed experimentally. These centers are the codimension of two singular points, where two bifurcations occur simultaneously. We observed two such singular points in our system: the multiplicity cusp point and the point where the Hopf and the SNP bifurcation lines meet (Figure 5). These organizing centers provide "defining conditions" for models, as any candidate model must be able to predict their existence. The coincidence of the saddle node and SNP is not a codimension two bifurcation, as the two occur for different points in the phase space. Note that some unobservable (unstable) codimension two singular points may also exist, for example, the intersection of unobservable Hopf and saddle-node bifurcations.

The analysis of the overall bifurcation behavior and the thermal imaging results provide guidance about the level of spatial complexity that a model must exhibit. At $\tau = 3.2$ s, the oscillations were caused by traveling temperature fronts which interacted with each other through the gas phase. A suitable model must account for the spatiotemporal variations of the surface concentrations and temperature and the gas-phase cou-

pling between distant surface elements. It may also be necessary to incorporate pacemakers into the activity profile of the surface (Imbihl et al., 1985). At the higher residence time of 6.4 s, the oscillations occurred uniformly and a less complex temporal model may be adequate.

Conclusions

Analysis of spatiotemporal temperature dynamics on a nickel disk during hydrogen oxidation revealed a rich variety of complex patterns whose characteristics changed dramatically with residence time. Thermal imaging results showed that at a residence time of 6.4 s, the oscillations were spatially uniform, while at a shorter residence time of 3.2 s, complex spatiotemporal temperature patterns developed. The reaction rate oscillations at the shorter residence time were due to traveling temperature fronts (both heating and cooling) which propagated from several pacemakers on the edge of the catalyst. During periodic oscillations, the fronts were emitted synchronously from the pacemakers, while during chaotic oscillations, the pacemakers were desynchronized and emitted waves independently of each other. Transport through the gas phase is the desynchronizing mechanism leading to nonuniform temperature patterns at the low residence time. The combination of thermal imaging and bifurcation analysis serves as a useful guide for developing candidate models of the system dynamics.

Currently the development, modeling and design of catalytic reactors are based on the assumption that the surface temperature of catalytic pellets is uniform. Clearly, the activity and selectivity of catalysts exhibiting spatiotemporal temperature patterns differ from those having a uniform temperature. Thus, it is important to gain a better understanding of the class of reactions and operating conditions under which spatial or spatiotemporal patterns exist. It is of particular interest to find out how common are these features under practical conditions, the magnitude of the error which is introduced by ignoring them, and under what conditions will the dynamics of individual catalytic pellets be synchronized and lead to global pattern formation in the reactor.

Acknowledgment

This work was supported by the National Science Foundation, the Welch Foundation, and the Energy Laboratory of the University of Houston. We wish to thank Prof. M. Sheintuch for many helpful discussions.

Notation

a_i = POD amplitude of mode i
a_v = surface to volume ratio of the catalyst
c_p = heat capacity of catalyst
C = feed concentration
h = heat-transfer coefficient
k = thermal conductivity of catalyst
L = characteristic length scale
T = gas temperature

Greek letters

λ_i = eigenvalue associated with φ_i
ρ = density of catalyst
τ = average residence time, characteristic time scale
φ_i = POD spatial mode i

Subscripts

f = feed
hs = thermal response of catalyst
O_2 = oxygen

Literature Cited

Belyaev, V. D., M. M. Slin'ko, V. I., Timoshenko, and M. G., Slin'ko, "Generation of Auto-Oscillations in the Hydrogen Reaction on Nickel," *Kinet. Kataliz*, **14**, 708 (1973).

Borckmans, P., G. Dewel, and A. DeWit, "The Search for Turing Structures: Success at Last?," *Seeds: Genesis of Natural and Artificial Forms*, Le Biopole Vegetal, Amiens (1990).

Brown, J. R., G. A. D'Netto, and R. A. Schmitz, "Spatial Effects and Oscillations in Heterogeneous Catalytic Reactions," *Temporal Order*, L. Rensing and N. Jaeger, eds., p. 86, Springer-Verlag, Berlin (1985).

Cox, M. P., G. Ertl, and R. Imbihl, "Spatial Self-Organization of Surface Structure during an Oscillating Catalytic Reaction," *Phys. Rev. Let.*, **54**, 1725 (1985).

Eiswirth, M., P. Moller, K. Wetzl, R. Imbihl, and G. Ertl, "Mechanisms of Spatial Self-Organization in Isothermal Kinetic Oscillations during the Catalytic CO Oxidation on Pt Single Crystal Surfaces," *J. Chem. Phys.*, **90**, 510 (1989).

Elmer, F. J., "Nonlinear and Nonlocal Dynamics of Spatially Extended Systems: Stationary States, Bifurcations and Stability," *Physica D*, **30**, 321 (1988).

Ertl, G., "Kinetics of Chemical Processes on Well-defined Surfaces," *Catalysis: Science and Technology*, Vol. 4, J. R. Anderson and M. Boudart, eds., p. 209, Springer, Berlin (1983).

Ertl, G., "Oscillatory Kinetics and Spatiotemporal Self-organization in Reactions at Solid Surfaces," *Science*, **254**, 1750 (1991).

Fink, T., R. Imbihl, and G. Ertl, "Excitation of Chemical Waves in a Surface Reaction by Laser-Induced Thermal Desorption: CO Oxidation on Pt(100)," *J. Chem. Phys.*, **91**, 5002 (1989).

Fukunaga, K., *Introduction to Statistical Pattern Recognition*, Academic Press, Boston (1990).

Graham, M. D., S. L. Lane, and D. Luss, "Proper Orthogonal Decomposition Analysis of Spatiotemporal Temperature Patterns," *J. Phys. Chem.*, **97**, 889 (1993).

Harold, M. P., M. Sheintuch, and D. Luss, "Analysis and Modeling of Multiplicity Features: 1. Nonisothermal Experiments," *Ind. Eng. Chem. Res.*, **26**, 786 (1987).

Imbihl, R., M. P. Cox, and G. Ertl, "Kinetic Oscillations in the Catalytic CO Oxidation on Pt(100): Experiments," *J. Phys. Chem.*, **84**, 3519 (1986).

Imbihl, R., M. P. Cox, G. Ertl, H. Muller, and W. Brenig, "Kinetic Oscillations in the Catalytic CO Oxidation on Pt(100): Theory," *J. Phys. Chem.*, **83**, 1578 (1985).

Jakubith, S., H. H. Rotermund, W. Engel, A. von Oertzen, and G. Ertl, "Spatiotemporal Concentration Patterns in a Surface Reaction: Propagating and Standing Waves, Rotating Spirals, and Turbulence," *Phys. Rev. Lett.*, **65**, 3013 (1990).

Kellow, J. C., and E. E. Wolf, "Infrared Thermography and FTIR Studies of Catalyst Preparation Effects on Surface Reaction Dynamics during CO and Ethylene Oxidation on Rh/SiO_2 Catalysts," *Chem. Eng. Sci.*, **45**(8), 2597 (1990).

Kellow, J. C., and E. E. Wolf, "Propagation of Oscillations During Ethylene Oxidation on a Rh/SiO_2 Catalyst," *AIChE J.*, **37**, 1844 (1991).

Kurtanjek, Z., M. Sheintuch, and D. Luss, "Surface State Kinetic Oscillations in the Oxidation of Hydrogen on Nickel," *J. Catal.*, **66**, 11 (1980).

Langmuir, I., "Chemical Reactions on Surfaces," *Trans. Faraday Soc.*, **17**, 607 (1921).

Lobban, L., and D. Luss, "Spatial Temperature Oscillations during Hydrogen Oxidation on a Nickel Foil," *J. Phys. Chem.*, **93**, 6530 (1989).

Lobban, L., G. Philippou, and D. Luss, "Standing Temperature Waves on Electrically Heated Catalytic Ribbons," *J. Phys. Chem.*, **93**, 733 (1989).

Lumley, J. L., *Stochastic Tools in Turbulence*, Academic Press, New York (1970).

Norton, P. R., "The Hydrogen-Oxygen Reaction on Metal Surfaces," *The Chemical Physics of Solid Surfaces and Heterogeneous Catalysis*, D. A. King and D. P. Woodruff, eds., p. 27, Elsevier, Amsterdam (1982).

Onken, H. U., and E. E. Wolf, "Coupled Chemical Oscillators on a Pt/SiO_2 Catalyst Disk," *Chem. Eng. Sci.*, **43**, 2251 (1988).

Pismen, L. M., "Kinetic Instabilities in Man-Made and Nature Reactors," *Chem. Eng. Sci.*, **35**, 1950 (1980).

Prigogine, I., and G. Nicolis, "On Symmetry-Breaking Instabilities in Dissipative Systems," *J. Chem. Phys.*, **46**, 3542 (1967).

Prigogine, I., and R. Lefever, "Symmetry Breaking Instabilities in Dissipative Systems," *J. Chem. Phys.*, **48**, 1695 (1968).

Sheintuch, M., "Asymmetric Surface States: A Source for Surface Reconstruction and Structure Sensitivity," *Chem. Eng. Sci.*, **36**, 893 (1981).

Schmitz, R. A., G. T. Renola, and P. C. Garrigan, "Observations of Complex Dynamic Behavior in the H_2-O_2 Reaction on Nickel," *Ann. NY Acad. Sci.*, **316**, 638 (1979).

Schmitz, R. A., G. T. Renola, and A. P. Zioudas, "Strange Oscillations in Chemical Reactions-Observations and Models," *Dynamics and Modelling of Reactive Systems*, W. E. Stewart, W. H. Ray, and C. C. Conley, eds., p. 177, Academic Press, New York (1980).

Schmitz, R. A., and T. T. Tsotsis, "Spatially Patterned States in Systems of Interacting Catalyst Particles," *Chem. Eng. Sci.*, **38**, 1431 (1983).

Sirovich, L., "Turbulence and the Dynamics of Coherent Structures: I, II and III," *Quart. Appl. Math.*, **XLV**, 561 (1987).

Sirovich, L., and C. H. Sirovich, "Low Dimensional Description of Complicated Phenomena," *Contemp. Math.*, **99**, 277 (1989).

Tsitsopoulos, L. T., and T. T. Tsotsis, "An Ellipsometric Investigation of Reaction Rate Oscillations during H_2 Oxidation on Ni," *Surf. Sci.*, **187**, 165 (1987).

Turing, A. M., "The Chemical Basis for Morphogenesis," *Phil. Trans. Roy. Soc.*, **B237**, 37 (1952).

Veser, G., F. Esch, and R. Imbihl, "Regular and Irregular Spatial Patterns in the Catalytic Reduction of NO with NH_3 on Pt(100)," *Catal. Lett.*, **13**, 371 (1992).

Zaikin, A. N., and A. M. Zhabotinskii, "Concentration Wave Propagation in Two-Dimensional Liquid-Phase Self-Oscillating System," *Nature*, **225**, 535 (1970).

Manuscript received Feb. 4, 1993, and revision received Apr. 26, 1993.